Available online at www.sciencedirect.com
SCIENCE DIRECT®
ELSEVIER
Journal of Nuclear Materials 320 (2003) 1–10
journal of nuclear materials
www.elsevier.com/locate/jnucmat

Techniques for tailored porosity in MgO targets

F. Valdivieso [a,*], P. Goeuriot [a], P. Matheron [b]

[a] *Céramiques Spéciales Department, SMS Center, URA CNRS 1884, 158 Cours Fauriel, Ecole Nationale Supérieure de Mines, F-42023 Saint-Etienne cedex 2, France*
[b] *CEA Cadarache, DENCAD-DEC-SPUA, F-13108 Saint-Paul-Lez-Durance, France*

Abstract

Four different processes to produce porous MgO have been studied; firstly, calcination of powders at several temperatures before forming by uniaxial pressing; secondly, effect compaction of powders at high mechanical isostatic pressure (400 MPa), followed by sieving and classical forming, addition of dopants, such as Li, Na and Al, and finally, a pressure gas sintering, even after long dwell times at high temperature (1700 °C/24 h). Densification during sintering has been studied. The microstructure evolution during stabilisation test, i.e. 1700 °C up to 24 h has also been characterised.

Thermal treatment of the powder does not permit a good dimensional stability of sintered samples, the shrinkage rate after 1 h at 1700 °C is about 0.2% min^{-1}. The addition of shrinkage delaying dopant (Li, Na) is not efficient, Al has a positive role, but depends on the addition process, the shrinkage rate after 1 h at 1700 °C is about 0.002% min^{-1}. The high pressure powder compaction has an intermediate effect (the rate of sintering is about 0.01% min^{-1}). Using a high gas pressure during sintering results in pores with flat surfaces, without re-densification during the 1 h treatment at 1700 °C. Nevertheless, the microstructure shows a grain growth.

1. Introduction

This work deals with studies about targets for long life fission products and minor actinides transmutation (Np, Cm, Am, ...). The latter, diluted in an inert matrix, still generate a high quantity of gas (mainly He), which leads to an important swelling of the material (the EFFTRA-T4 experiment has recently shown 18 vol.% change in an $MgAl_2O_4$ matrix). This study is based on the innovative concept of a porous matrix permitting far elimination of gases to the plenums as and when they are produced, to avoid geometrical modifications. The objective is to get a microdispersion of fissile material (<30 vol.% (Am, Cm)O_2) into a porous magnesia matrix, whose main qualities are:

- small grains, in order to limit the diffusion length to pores,
- small pores, to increase the number of diffusion paths,
- high open porosity rate,
- thermal stability of porosity to avoid densification in pile for temperatures < 1600 °C.

A lot of theoretical and experimental studies of different stage sintering have dealt on the elimination of the porosity, in order to control the final microstructure of the material [1–4]. Nevertheless, there is a narrow relation between the initial density, the agglomeration of the powder, the grain distribution size and the pore size with the microstructure evolution during sintering and the final density. Therefore, the mastering of these parameters permits the control of the final microstructure. So, Zhao and Harmer [5] and Zheng and Reed [6] have shown that a broad pore size distribution, due to agglomeration or poor consolidation, leads to sintering difficulties. Thus, smaller pores, higher densities, and narrow pore size distribution are precursors to rapid sintering densification and high densities [7].

Nevertheless, in the final stage of sintering, when the pores close, this evolution is connected to the relation

* Corresponding author. Tel.: +33-4 77 42 0083; fax: +33-4 77 42 0249.
E-mail address: francois.valdivieso@emse.fr (F. Valdivieso).

0022-3115/03/$ - see front matter © 2003 Elsevier Science B.V. All rights reserved.
doi:10.1016/S0022-3115(03)00161-2

between the mobility of porosity with the mobility of grain boundary [8,9], based on kinetics considerations. The microstructural evolution diagram of grain size versus pore size shows the pore–boundary interaction when the migration of pores is limited by surface diffusion. Thus, with this diagram one can see there is a limit where the pores and boundary have the same mobility; therefore the microstructure is stable. Nevertheless, this limit can be modified by impurities [10,11], and also by the pore size distribution [12]. To summarize, the analysis of the pore–boundary interaction and its representation in terms of the grain size versus pore size diagram requires simplifications and assumptions. They provide a useful basis for qualitative understanding of microstructural control in the final stages of sintering. However, they cannot be used to predict quantitatively the microstructural evolution of real systems.

The thermodynamics of interaction must also be considered because it determines whether a pore will shrink or grow during sintering. Actually, the equilibrium pore shape is dictated by the dihedral angle ψ defined by $\cos(\psi/2) = \gamma_{gb}/2\gamma_{sv}$, where γ_{sv} and γ_{gb} are the interfacial tensions at the pore surface and the grain boundary interface, respectively. Kingery and François [2] using geometrical consideration have shown there is a relation between the dihedral angle and the number of sides of a closed pore (or the grain growth). Thus, pores with a concave curvature are unstable and shrinks; pores with a convex curvature also are unstable but they grow, and finally pores with plane surfaces are stable.

If these thermodynamic or kinetic considerations about the stability of porosity have been established for pores closed in materials, only modelling of the kinetics of the elimination of porosity have been studied in the intermediate stage of sintering, where the porosity is open [13,14].

The aim of the present work is to determine experimentally the preparation of a porous material, based on magnesia. The porosity should be at the limit of open-closed porosity, i.e. between 90% and 94% TD, and stable after heat treatment. Different ways have been investigated.

- The powder is fired for a long time and at different temperatures to promote grain growth and larger pores after sintering.
- Dopants have been added to assist or to delay the sintering process.
- Hard, poorly deformable agglomerates have been generated to introduce differential sintering during the stage of firing, and consequently a large porosity around these agglomerates.
- Sintering under a high pressure of gas (gas pressure sintering) has been tested to diminish the sintering and improve the stability of the pores.

The stability of pellets, is compared to the dense material (Al_2O_3, 99.9% d_{th}) submitted to a same test, i.e. 1700 °C/1 h.

2. Experimental procedure

2.1. Samples preparation

Magnesium oxide powder (CERAC M 1017, 99.95% purity) was pelletised at various pressures (60 or 170 MPa) using a double effect uniaxial press. In order to produce calibrated agglomerates with higher density, isostatic pressing was used: A quantity of powder was pressed at 400 MPa, then the compact obtained was crunched in an agate bowl and was sieved at 100 or 200 μm. Then, the pellet was pressed with this powder using a uniaxial press (60 or 170 MPa).

The addition of small quantities of Li_2CO_3, Na_2CO_3 and γ-Al_2O_3 was made by dry mixing in a turbula. These oxides were added by successive dilutions with MgO powder, in order to perform 1 wt% of additional oxide (Li_2O, Na_2O or Al_2O_3) in the MgO matrix; the total time of mixing was 1 h.

Before sintering, the compacted samples were submitted to a thermal treatment from room temperature to 800 °C at a rate of 200 °C h^{-1}, under dynamic vacuum conditions (primary vacuum), then stocked in a drying oven at 120 °C, in order to prevent their hydration before sintering.

The pressureless sintering of the samples was performed in a furnace, under air conditions, at a rate of 200 °C h^{-1} up to the determined temperature. Another device used to improve the shrinkage of the samples was the gas pressure furnace (G.P.S, FPW 100/150-2200-100 AS, KCE Sondermaschinen, Germany). It has two modes of operations, the pressure of nitrogen gas was controlled and increased concurrently with the temperature from 0.1 to 6.5 MPa. In the second mode, the pressure of the gas was maintained at 6.5 MPa during all the time of the cycle of temperature. Table 1 summarises all powders and samples prepared and their corresponding names (a letter in this case).

2.2. Sample characterisation

The sinterability of samples was characterised by dilatometry (TMA 92-17, SETARAM) on samples with initial dimensions of 6 mm height and a diameter of 8 mm.

The dimensional stability of sintered specimens was characterised, also following a standard procedure, i.e. the dilatation or shrinkage is recorded during a thermal cycle of 200 °C h^{-1} up to 1700 °C followed by a dwell of 1 h (in some cases up to 4 and 24 h). The rate of shrinkage at the end of the dwell was the parameter

Table 1
Powders prepared in this study

Name	Treatment of the powder	Type of sintering
A	Raw MgO powder	Pressureless in air or gas pressure sintering
B	MgO powder fired at 1000 °C during 16 h, in air	Pressureless in air
C	MgO powder fired at 1000 °C during 40 h, in air	Pressureless in air
D	MgO powder fired at 1300 °C during 30 h, in air	Pressureless in air
E	MgO pellet fired at 1300 °C during 30 h, in air	Pressureless in air
F	MgO powder, isostatic compression at 400 MPa, then sieved at 200 μm	Pressureless in air
G	MgO powder, isostatic compression 400 MPa, sieved at 200 μm, and then mixed with 1 wt% γ-Na_2CO_3 in turbula	Pressureless in air
H	MgO powder, isostatic compression at 400 MPa, sieved at 200 μm, and then mixed with 1 wt% γ-Al_2O_3 in turbula	Pressureless in air
I	MgO powder, isostatic compression at 400 MPa, sieved at 200 μm, and then mixed with 1 wt% γ-Li_2CO_3 in turbula	Pressureless in air
J	MgO powder mixed with 1 wt% γ-Al_2O_3 in turbula, compacted at 400 MPa, and then sieved at 100 μm	Pressureless in air or gas pressure sintering
	MgO powder mixed with 1 wt% γ-Al_2O_3 in turbula, compacted at 400 MPa, and then sieved between 100 and 200 μm	Pressureless in air or gas pressure sintering
L	MgO powder, compacted at 400 MPa, sieved at 100 μm, and then mixed with 1 wt% γ-Al_2O_3 in turbula	Pressureless in air or gas pressure sintering
M	MgO powder, compacted at 400 MPa, sieved between 100 and 200 μm, and then mixed with 1 wt% γ-Al_2O_3 in turbula	Pressureless in air or gas pressure sintering
N	MgO powder mixed with 1 wt% γ-Al_2O_3 in turbula	Pressureless in air

chosen to evaluate the dimensional stability of samples. This rate was compared with shrinkage rate of a pure alumina sample (99.9% d_{th}), named reference sample.

The density of samples was measured using Archimedes method in alcohol (99.95%). To characterise the porosity the specimens have been fractured or cut in order to observe respectively, with an electron microscope (JEOL JSM 840), the morphology of the porosity and its evolution inside the material.

3. Results and discussion

3.1. Effect of thermal process of powder on reactivity

The initial magnesia powder has a coarse granulometric distribution and large agglomerates, of a few tens of microns. These agglomerates are constituted of fine (100–200 nm) particles (Fig. 1). Thus the system, with fine particles and consequently fine porosity, has a good reactivity during the sintering cycle. In order to suppress this reactivity, and form large pores in the compact, that will be more stable, the powder has been thermally processed at two temperatures. The treatment was made at 1000 °C, where no shrinkage mechanism is observed, for 16 and 40 h, or at 1300 °C where a small densification is observed (see Fig. 2). At lower temperatures

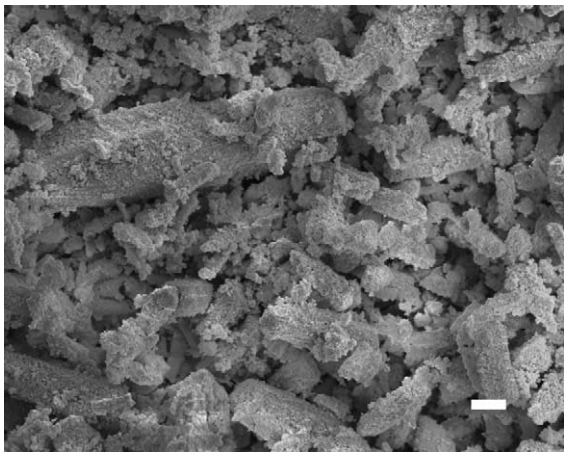

Fig. 1. Raw MgO powder (A) (bar = 10 μm).

(1000 °C) no difference with the raw powder was observed.

Fig. 3 shows the dilatometry curves obtained from compacted pellets from the powders A, B, C and D. It appears clearly that the densification is affected by the different treatments, even though the powders have not shown visual differences, apart from powder D. Actually, the densification begins at higher temperatures, for the thermally heated powders. Also, the reactivity of

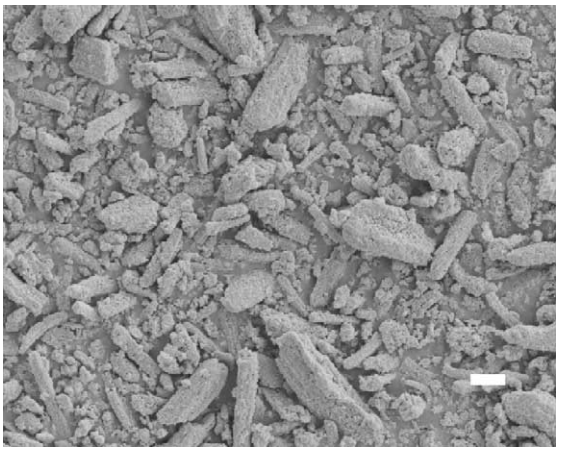

Fig. 2. Powder fired at 1300 °C during 30 h (D) (bar = 10 μm).

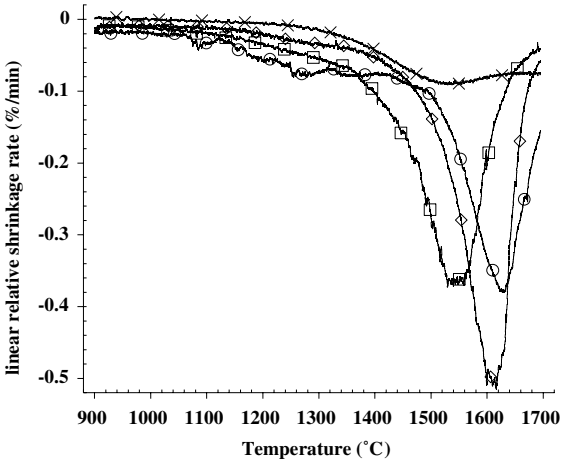

Fig. 3. Linear relative shrinkage rate versus temperature: for powders (○) A, (□) B, (◇) C and (×) D.

powder D, heated at 1300 °C for 30 h, is strongly reduced, the maximum relative shrinkage rate is about a fourth of that for the other powders.

The samples sintered from powders A, B and C densify to 85% TD, while the sample obtained with powder D only reaches 65% TD. The final density can be adjusted by controlling the temperature of thermal treatment on the powder. For an effective effect this treatment must be performed in a temperature range where the powder starts to shrink. However, even if the shrinkage has been sharply inhibited, as for D, at the end of the sintering cycle the linear relative shrinkage rate stays higher, 0.03% min^{-1}, whereas in the cases where the shrinkage has been slowly delayed 0.01% min^{-1}, for powders A, B, C (Fig. 4).

So, the shrinkage rates following a 1 h dwell at 1700 °C are significantly higher compared with the

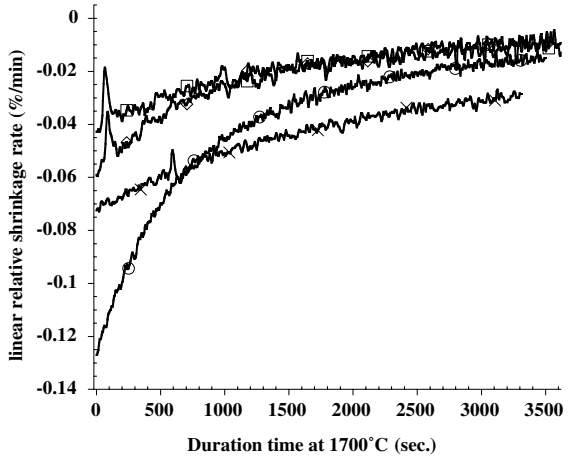

Fig. 4. Linear relative shrinkage rate versus temperature during the dwell of temperature at 1700 °C in air: (○) A, (□) B, (◇) C and (×) D.

sample reference, Al_2O_3 99.9% TD (0.0015% min^{-1}). As a consequence, these different systems will present density evolution. Fig. 5 shows the difference in the sintering behaviours between a powder and a compact heated at 1300 °C during 30 h. Sample E is a pellet which has been pressed at 56 MPa then heated at 1300 °C for 30 h, while sample D is a pellet pressed at 56 MPa realised with a powder heated in the same thermal cycle.

During the thermal pre-treatment stage, the densification between particles is more important in pelletised samples than in powders, consequently the densification rate in sample E is higher than D, before sintering at 1700 °C. After sintering, sample E has a higher shrinkage rate than sample D. Also the density is higher, 65% and 83% TD, respectively. Consequently, the heat treatment, as expected, has more influence on the reactivity of the powder than on the pressed powder.

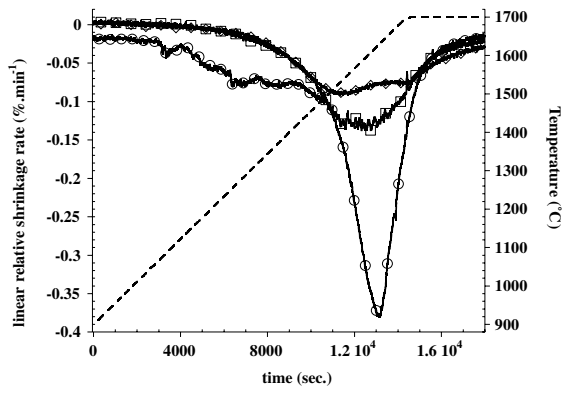

Fig. 5. Linear relative shrinkage rate versus temperature: for samples (○) A, (◇) D and (□) E.

Never- theless, because of low densification rate (on sample D) the system presents a relative evolution more significant than sample E. In spite of a lower relative shrinkage rate, in sample E, at the end of sintering (after the dwell at 1700 °C), it is similar to that obtained with raw powder, but still too high.

3.2. Effect of forming pressure

The heat treatment inhibits the reactivity of the system, but leading to poor densification rate, and an insufficiently stable system. In order to prevent further densification during the dwell at 1700 °C, the samples have been pressed with two different methods: to increase the reactivity of the system and enhance the final density, to obtain more stable sintered samples.

3.2.1. Effect of compaction pressure

Fig. 6 shows the shrinkage behaviour of two samples of untreated MgO powder (A), pelletised at 56 and 170 MPa. The maximum relative shrinkage rate is higher for samples, pressed at low pressure, because of the low initial density, 41% TD versus 50% TD. During the dwell at 1600 °C, the rate nears zero more rapidly when the green density was the highest. However, the final densities are the same, about 88% TD, because of the long time dwell. The compaction at a higher pressure (or initial density) improves significantly a better final density, and therefore the linear relative shrinkage rate is reduced quantitatively to 0.008% min^{-1} (Fig. 7). Nevertheless, the dwell at 1600 °C for 4 h, could play a major rule in the stabilisation of densification. Therefore, at once the duration dwell at high temperature and a high pressure of forming can lead to reasonable materials. Unfortunately, in this study the relative shrinkage rate, at the end of the dwell temperature at 1700 °C, is low (0.008% min^{-1}) but too high compared to the standard sample.

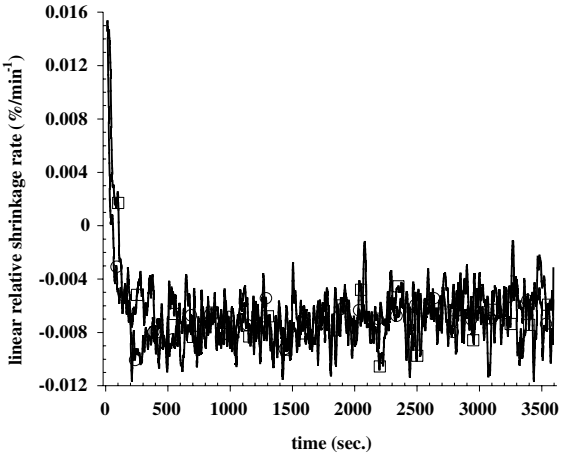

Fig. 7. Linear relative shrinkage rate versus time at 1700 °C for samples pressed at (○) 56 MPa and (□) 170 MPa.

3.2.2. Effect of isostatic pre-compaction

Fig. 8 shows the linear relative shrinkage rate during the standard temperature cycle (200 °C h^{-1} up to 1700 °C, and a dwell of 1 h) for samples compacted at 56 MPa with the raw powder A and the sample also compacted at 56 MPa but with powder F, which is a powder having undergone pre-compaction at 400 MPa, and then sieved at 200 μm. It appears clearly that the maximum of the relative rate is lowered by 150 °C, due to a better contact between the particles in the agglomerates.

Also, the sintering of sample F is finished, long before sample A. At 1600 °C the relative shrinkage rate is yet near zero, and after 1 h at 1700 °C its value is 0.008% min^{-1}, and its relative density was 89.2% TD.

3.3. Effect of doping and pressure

The pre-compaction powder stage seems to be an excellent process in order to improve the sinterability of

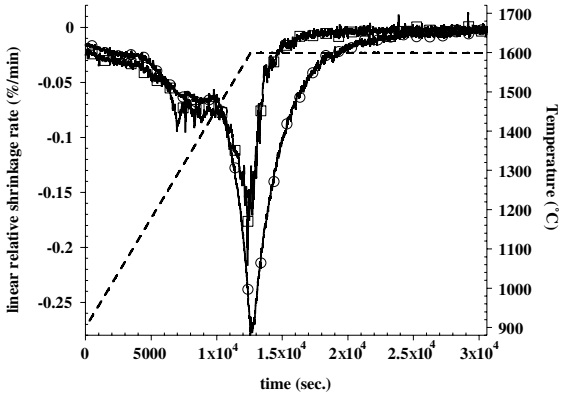

Fig. 6. Effect of pressure of compaction on sinterability of powders A, pressed at (○) 56 MPa and (□) 170 MPa.

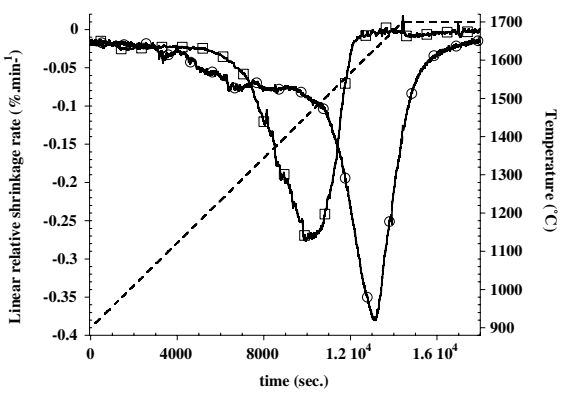

Fig. 8. Effect of compaction of the raw powder on sintering: (○) A powder and (□) F powder.

the samples. However, for the same sintering cycle the densification rate is not very improved compared to the case where the powder is simply pressed.

Another way to improve the densification is to influence the point defect concentration in the compact powder. In fact, an increase in defect concentration can result in faster sintering. In the case of MgO, it is known well [15] that the intrisic defects are Schottky defects, i.e. oxygen and magnesium vacancies, and the sintering is controlled by the diffusion of oxygen vacancies. Thus, the addition of cations with charge lower than +2 will act to increase the sintering rate, whereas the addition of cations with charge higher than +2 will inhibit it. Thus, NaF and particularly LiF can positively adjust the ionic vacancy, whereas Al_2O_3 would act as an inhibitor.

3.3.1. Effect of doping process by γ-alumina on microstructure

Figs. 9 and 10 show the difference in microstructure between sample N prepared from MgO powder mixed with 1 wt% of γ-alumina and sample H which was prepared from the mixture of 1 wt% of γ-alumina with MgO powder compacted at 400 MPa and then sieved at 200 μm. It appears that porosity is concentrated around small aggregates in sample N and around large agglomerates in case where alumina has been added to dense agglomerates. The presence of γ-alumina leads to an absence of densification compared to agglomerates which are free from it. After sintering the relative densities of samples H and N are respectively 90.7% and 85.2% TD. On other hand, it seems when the alumina is mixed to raw powder before compaction (at 400 MPa) the sintering is delayed compared to the case where the alumina is mixed after the compaction, i.e. at the surface of agglomerates. It is impossible to conclude on the efficiency of γ-alumina addition, because

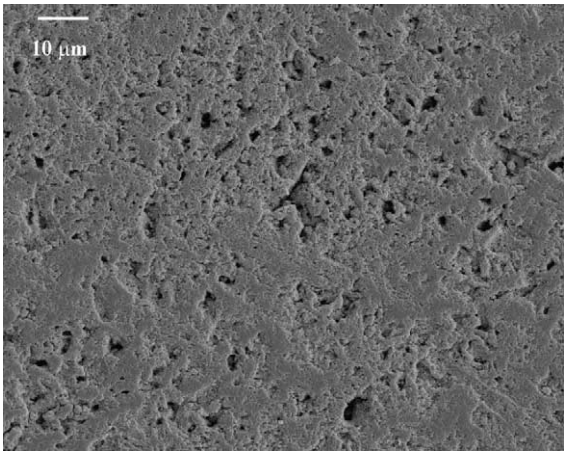

Fig. 9. Polished surface of sample N.

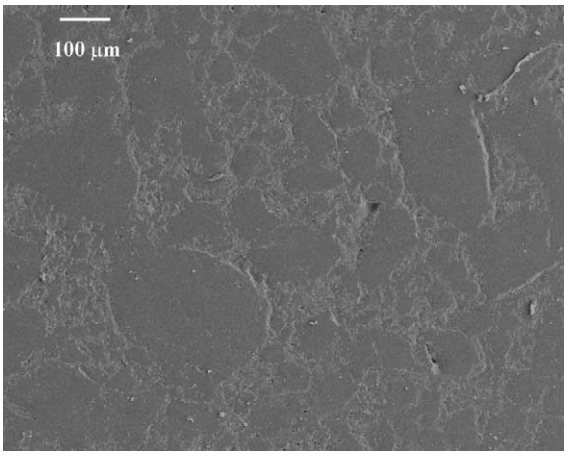

Fig. 10. Polished surface of sample H.

compared to raw powder (A) the final relative density is comparable. But, for sample H the relative densification rate at the end of dwell is only 0.003% min^{-1}, near to the standard sample (pure and dense alumina sample).

3.3.2. Doping by γ-alumina, Li_2CO_3 or Na_2CO_3

Fig. 11 shows the linear relative shrinkage rate of four types of samples: Sample G with addition of Na_2CO_3 to the powder pre-compacted at 400 MPa and sieved at 200 μm, sample H with γ-Al_2O_3 addition after the same process and finally sample I with Li_2CO_3 addition. For these three powders 1 wt% of oxides has been added. Their sintering behaviour is compared to raw material compacted at 400 MPa and then sieved at 200 μm (F). All samples present a high reactivity compared with sample F, the maximum rate of shrinkage

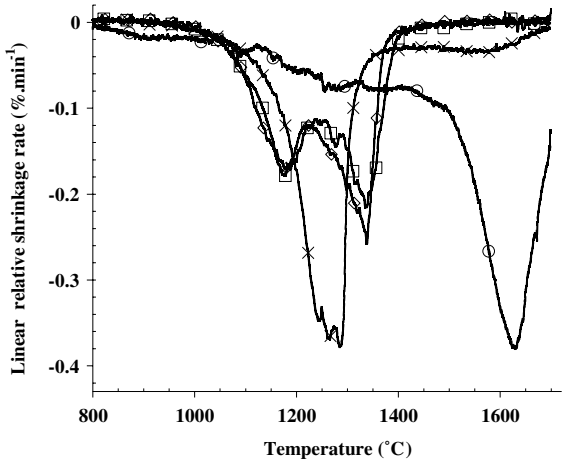

Fig. 11. Effect of dopant addition on sintering: (○) F, (□) G (Na^+), (◇) H (Al^{3+}) and (×) I (Li^+) powders.

significantly advanced. Clearly, Na or Al addition has the same effect on rate of sintering: two peaks appear at 1160 and 1350 °C, while at 1500 °C their rates are near zero. In the case of Li addition, one single peak appears, at an intermediate temperature (1275 °C), but with a higher intensity. So, after a rapid deceleration of shrinkage, the rate remains constant with a value about 0.03% min^{-1} from 1400 °C up to 1600 °C. Above this temperature, the rate decreases near the values obtained with other additives. Thus Li has a good capability to enhance sintering until high temperatures, compared to other additives.

After sintering (1700 °C/1 h, in air) the relative densities were 85.3%, 87.8% and 85.8% TD for G, H and I samples respectively. After the heat treatment some variations of densities are noted: whereas a minor re-densification is observed on the sample doped with Al (88.9% TD), both dopants with a lower cationic charge, lead to a high re-densification, 90.3% for Na addition and 90.8% TD for Li addition, respectively.

3.3.3. Effect of doping process and classification

For γ-alumina addition, Fig. 12 shows the shrinkage rate evolution during sintering of four powders (J, K, L and M, see Table 1). These results are compared to the powder simply compacted at 400 MPa (F). As observed earlier, the addition of small quantities of γ-alumina lead to a better reactivity in the compact sample.

The powders which have been sieved under 100 μm (J and L) start their shrinkage earlier than powders sieved between 100 and 200 μm (K and M), even though they have the same initial density, 55% TD. As powders J and L have a large particle size distribution from primary crystallite to agglomerates of 100 μm, their reactivity is higher than agglomerates of 100–200 μm present in K and M powders. Moreover, for the larger agglomerates (K and M), if the γ-alumina is inside instead of around the agglomerates, the shrinkage starts later. Thus the best sintering inhibition by the Al dopant occurs when it is dispersed in the MgO matrix rather than around the agglomerates. After the sintering cycle, all samples have the same density, 87.5% TD. If we compare to sample H (obtained without classification) it appears that is not necessary to use a powder with a narrow granulometric distribution in order to obtain the best relative density after sintering.

During the test of re-densification all compositions show the same behaviour (Fig. 13). The linear relative shrinkage rate is relatively constant and very low during the dwell at 1700 °C, about 0.002% min^{-1}. Table 2 shows the evolution of the densification of the samples sintered in air, and after heat treatment (1700 °C/1 h). As previously observed in Fig. 12, the samples with γ-alumina added, sieved below 100 μm (J), showed a higher densification compared to samples sieved over 100 μm (K). Moreover, when γ-alumina is added to agglomerated powder (obtained by compaction, L and M), the densities are lower than obtained with γ-alumina added directly to the raw powder (J and K respectively). The alumina is more efficient in its role of shrinkage inhibitor, when it is located over agglomerate surfaces. The intra-agglomerate sintering is possible but the inter-agglomerate sintering is inhibited by a higher concentration of γ-alumina between the agglomerates. After heat treatment, the densities vary a little, except for L and M compositions. We can see here that the control of the process of γ-alumina addition and of the agglomerate size distribution can allow us to adjust the final density, with a good dimensional stability at high temperatures (for H, J and K samples).

Table 2 shows the densification rate after sintering and re-heating of sample H, which has a large particle

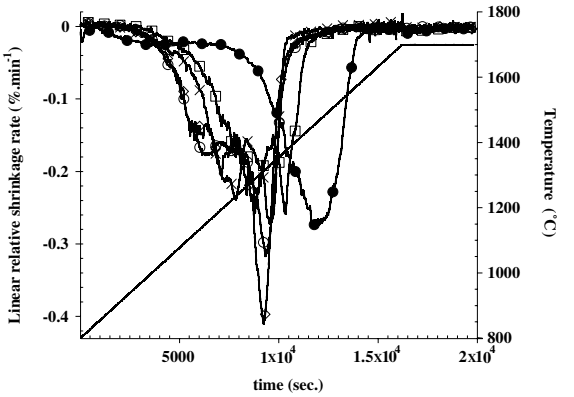

Fig. 12. Effect of sieving and process of the addition of γ-Al_2O_3 on the sintering: (●) F, (○) J, (□) K, (◇) L and (×) M.

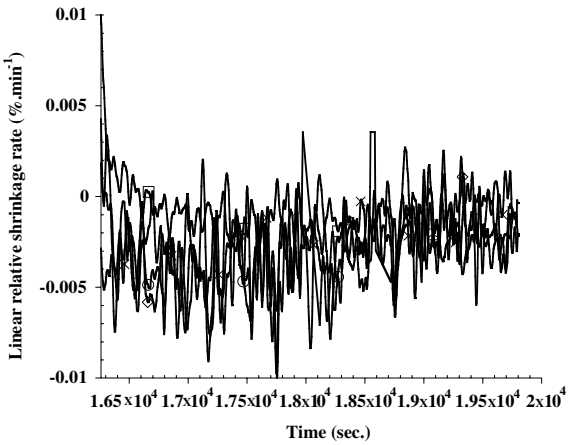

Fig. 13. Linear relative shrinkage during the test of stability at 1700 °C: (○) J, (□) K, (◇) L and (×) M.

Table 2
Effect of doping process by γ-alumina combined with sieving on the densification

	H	J	K	L	M
Density of green samples (% TD)	52.2	51.1	49.7	51.9	51.4
Density after pressureless sintering (% TD)	87.8	88.6	83.6	83.6	82.2
Density after heat treatment (% TD)	87.5	88.6	84.4	86.1	84.0

size distribution. It appears for this sample H that the final density is higher and its variation after heat treatment is comparable to previous powders.

3.3.4. Effect of doping and gas pressure during sintering

In order to promote a large porosity, samples have been sintered from powders A, G, H and I (see Table 1), under gas pressure conditions. In the first case the gas pressure (N_2) was increased linearly, parallel to the temperature from 1000 to 1700 °C, at 0.03 MPa min^{-1}. The results of densities are presented in Table 3. When dopants are added, and specially with γ-alumina (H), the inhibitor effect is really marked, the density is about 6% less than other samples. It seems that the pressure has inhibited the activator effect of sintering with Li (I) and Na (G) dopants. Actually, even after heat treatment all samples show a little bit densification, and specially the samples doped with Li or Na present a very weak evolution.

In the second case, the gas pressure (N_2, 6.5 MPa) was held constant from room temperature to the end of the sintering cycle. The results of densification are presented in Table 4. Except for sample H powder (Al doped), all other samples show a lower densification compared to the case where the pressure was continuously increased. When gas pressure is high during all cycle, it appears that the activator or inhibitor mechanism of the sintering due to doping are not effective. In this case during heat treatment, no shrinkage is observed even for the dwell of temperature at 1700 °C.

3.4. Microstructure evolution

Fig. 14 shows the evolution of microstructures during re-heating at 1700 °C after 4 and 24 h of treatment, compared to the as-sintered conditions. Sample A sintered under gas pressure conditions is constituted of fine particles, ~3 μm (Fig. 14(a)); the porosity seems to be well distributed around the grains. As the thermal treatment time increases (Fig. 14(b) and (c)) the pore size and the grain size increase. Nevertheless a large majority of the porosity remain at the triple point. After 24 h at 1700 °C, the grain size is about 8 μm; it is a size slightly greater than that obtained at 4 h, and once again the pore size has increased, but less than after 4 h. During re-heating treatment, the grain boundaries begin to flatten. In such conditions the porosity will stay stable for a longer time.

Fig. 15(a)–(c) shows the microstructure evolution of a sample which has been prepared with raw powder mixed with 1 wt% of γ-alumina (N), and sintered in air at 1700 °C/1 h. After sintering (Fig. 15(a)) the grain size is larger than the one obtained with gas pressure sintering on sample A.

The grains are less flat, but become rounded, and the porosity is also well dispersed around the grains and

Table 3
Effect of additives on the density, after gas pressure sintering (P_{N_2} linearly increasing with temperature), at 1700 °C/1 h, and after heat treatment at 1700 °C during 1 h in air

	A	G	H	I
Density of pressureless sintered samples (% TD)	85.0	85.3	87.8	85.8
Density after gas pressure sintering (N_2) (% TD)	85.0	84.4	78.9	85.6
Density after heat treatment at 1700 °C, during 1 h in air (% TD)	85.8	84.6	80.3	85.8

Table 4
Effect of additives on the density, after gas pressure sintering (P_{N_2} is constant 6.5 MPa) at 1700 °C/1 h under and after heat treatment at 1700 °C during 1 h in air

	A	G	H	I
Densification rate of pressureless sintered samples (% d_{th})	85	85.3	87.8	85.8
Densification r after gas pressure sintering (P_{N_2} constant) (% d_{th})	81.9	79.7	81.7	79.4
Densification r after heat treatment à 1700 °C, during 1 h in air	81.9	–	81.4	–

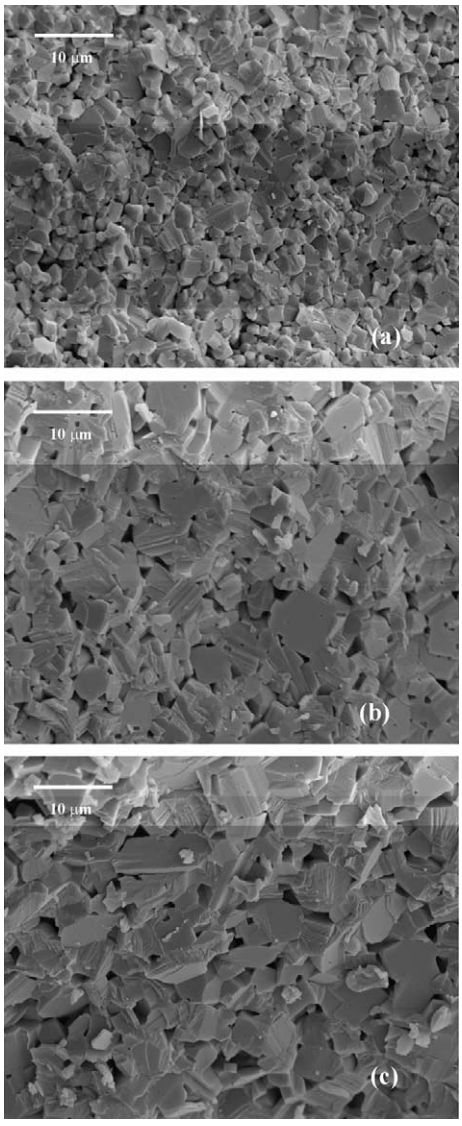

Fig. 14. Microstructure evolution during the heat treatment on sample A: (a) as sintered sample, (b) after 4 h at 1700 °C and (c) after 24 h at 1700 °C.

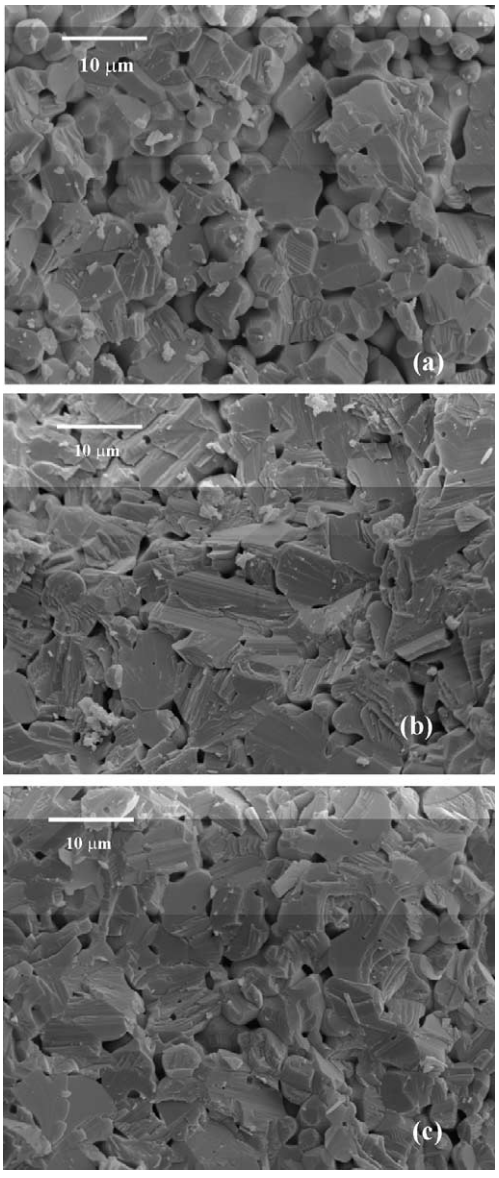

Fig. 15. Microstructure evolution during the heat treatment on sample N: (a) as sintered sample, (b) after 4 h at 1700 °C and (c) after 24 h at 1700 °C.

seems to be open. During heat treatment, after 4 h the grains grew slightly and the pore size strongly decreased (Fig. 15(b)). Beyond 4 h, the microstructure shows weak grains size increase, but the total porosity seems to remain constant

When the alumina is located around the agglomerates compacted at 400 MPa, the microstructure is constituted by dense agglomerates of very large size. The porosity distribution in these agglomerates is shown in Fig. 16(a)–(c). It is essentially closed in the very dense agglomerates. Most of the porosity is inter-agglomerate and its size is very large (several microns) due to differential sintering between agglomerates. No significant evolution of the porosity is quantified for the high temperature treatment.

The figures show that the microstructure evolves during heat treatment. When the powder is not compacted at high mechanical pressure, the porosity coalesces to form large pores and the grains grow too. So, when gas pressure is used the growth is limited during sintering, but after heat treatment the grain size is comparable to that obtained in pressureless sintering with γ-alumina addition. Indeed when the powder is

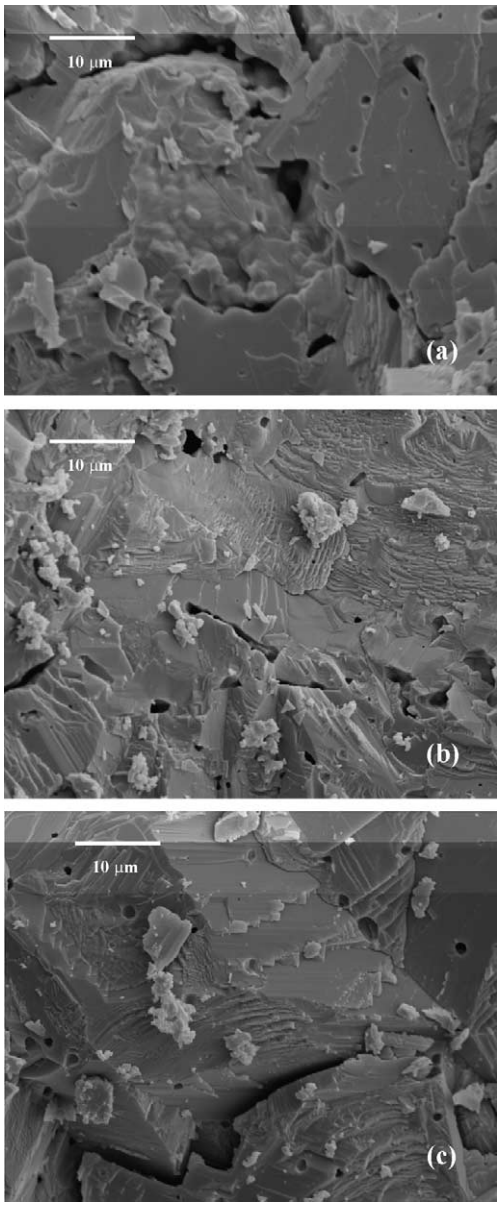

Fig. 16. Microstructure evolution during the heat treatment on sample H: (a) as sintered sample, (b) after 4 h at 1700 °C and (c) after 24 h at 1700 °C.

initially compacted (at 400 MPa) the density of sintered samples do not vary during re-heating but the porosity is concentrated around large agglomerates.

4. Conclusion

Among the four processes investigated to prepare a material with large and a stable porosity at very high temperature, some answers or ways have been found. The isostatic compaction of powders before forming allows to advance the sinterability of materials to lower temperatures, and the consequence is a better stability of relative dense pellets at a high temperature (1700 °C/1 h or more), but not sufficient. The addition of γ-alumina has appeared as a good inhibitor of sintering, and leads to a better stability of the densification rate, with the best compromise leading to a rate of 0.002% min^{-1}.

The gas pressure sintering, with a constant pressure during sintering, allows us to introduce pores with a larger size, this size evolves mainly during the stabilisation test until four hours of treatment. All samples sintered for 1 h at 1700 °C have shown a slight evolution (relative density or microstructure) for the four first hours, and then a good relative stability. Nevertheless, the relative density of the material, in this case MgO powder uniaxially pressed, is not affected, and no doping is necessary. One can think that a four hour long dwell would allow us to obtain the microstructure with the best compromise, either with gas pressure sintering or with pressureless sintering but with γ-alumina addition. This work, conducted only with MgO matrix, is actually being continued, trying to incorporate a fissile phase ($(Pu, Ce)_2Zr_2O_7$), where cerium simulates americium.

Acknowledgements

It is a pleasure to thank Dr F. Sudreau and C. Perrais (CEA Cadarache, France) for the helpful discussions during the various stages of this work.

References

[1] E.B. Slamovitch, F. Lange, J. Am. Ceram. Soc. 75 (1992) 113.
[2] W.D. Kingery, B. François, in: G.C. Kuczynski, N.A. Hooton, G.F. Gibbon (Eds.), Sintering and Related Phenomena, Gordon and Breach, New York, 1967, p. 471.
[3] R.J. Brook, in: F.F.W. Wang (Ed.), Ceramic Fabrication Processes, Treatise on Materials Science and Technology, vol. 9, Academic Press, New York, 1976, p. 331.
[4] B.J. Bellet, F.F. Lange, J. Am. Ceram. Soc. 71 (1988) 71.
[5] J. Zhao, M.P. Harmer, J. Am. Ceram. Soc. 71 (1988) 113.
[6] J. Zheng, J.S. Reed, J. Am. Ceram. Soc. 72 (1989) 810.
[7] T.S. Yeh, M.D. Sacks, J. Am. Ceram. Soc. 71 (1988) 484.
[8] R.J. Brook, J. Am. Ceram. Soc. 52 (1969) 339.
[9] F.A. Nichols, J. Appl. Phys. 37 (1966) 4599.
[10] R.J. Brook, J. Am. Ceram. Soc. 52 (1969) 56.
[11] K.A. Berry, M.P. Harmer, J. Am. Ceram. Soc. 69 (1986) 143.
[12] J. Zhao, M.P. Harmer, J. Am. Ceram. Soc. 71 (1988) 530.
[13] R.L. Coble, J. Appl. Phys. 32 (1961) 787.
[14] R.L. Coble, J. Appl. Phys. 32 (1961) 793.
[15] M.N. Rahaman, in: Ceramic Processing and Sintering, Marcel Dekker, New York, 1995.